Electrochemically Determined, and Structurally Justified Thermochemistry of H-atom Transfer on Ti-Oxo Nodes of the Colloidal Metal–Organic Framework, Ti-MIL-125

*Nazmiye Gökçe Altınçekiç,† Chance W. Lander,† Ayman Roslend,‡ Yihan Shao,† and Hyunho Noh†**

†Department of Chemistry and Biochemistry, The University of Oklahoma, Norman, OK 73019, USA

‡Department of Chemistry, Northwestern University, Evanston. IL 60208, USA

ABSTRACT: Titanium dioxide (TiO_2) has long been employed as (photo)electrodes for reactions relevant to energy storage and renewable energy synthesis. Proton-coupled electron transfer (PCET) reactions with equimolar amounts of protons and electrons at the TiO_2 surface or within the bulk structure lie at the center of these reactions. Because a proton and an electron are thermochemically equivalent to an H-atom, these reactions are essentially H-atom transfer reactions. Thermodynamics of H-atom transfer has a complex dependence on the synthetic protocol and chemical history of the electrode, the reaction medium, and many others; together, these complications preclude the understanding of the H-atom transfer thermochemistry with atomic-level structural knowledge. Herein, we report our success in employing open-circuit potential (E_{OCP}) measurements to *quantitatively* determine the H-atom transfer thermochemistry at structurally well-defined Ti-oxo clusters within a colloidally stabilized metal–organic framework (MOFs), Ti-MIL-125. The free energy to transfer H-atom, $Ti^{3+}O$–H bond dissociation free energy (BDFE), was measured to be 68 ± 2 kcal mol^{-1}. To the best of our understanding, this is the first report on using E_{OCP} measurements on any MOFs. The proton topology, the structural change upon the redox reaction, and BDFE values were further *quantitatively* corroborated using computational simulations. Furthermore, comparisons of the E_{OCP}-derived BDFEs of Ti-MIL-125 to similar parameters in the literature suggest that E_{OCP} should be the preferred method for quantitatively *accurate* BDFE calculations. The reported success in employing E_{OCP} for nanosized Ti-MIL-125 should lay the ground for thermochemical measurements of other colloidal systems, which are otherwise challenging. Implications of these measurements on Ti-MIL-125 as an H-atom acceptor in chemical reactions and comparisons with other MOFs/metal oxides are discussed.

INTRODUCTION

Redox reactions at the interface of the catalyst and the surrounding solution are prevalent in nearly all chemical transformations relevant to the energy and chemical sectors.[1-3] Many of these reactions involve a transfer of hydrogen atoms (H-atoms) between the substrate/product and the catalyst surface.[4-8] In thermal catalysis like hydrogenation, for example, the initial step involves a homolytic cleavage of H_2 to form a reactive surface H-atom (eq. 1). Surface adsorption process is emphasized by the explicit denotation of the adsorption site (*S*) as the reaction substrate. The catalyst-adsorbed H-atom, *S*–H, can react with a generic substrate, X, to form the product, X–H (eq. 2); the reverse is the case for a dehydrogenation reaction.[8-10] In photo- and electrocatalysis, the surface-bound H-atoms are often a product of interfacial proton-coupled electron transfer (PCET) reactions involving equal amounts of protons and electrons (eq. 3). The surface-bound H-atoms are critical intermediates for the reactions of H_2, O_2, CO_2, N_2, and many others (eqs. 4-7).[1,3,4,11,12] Intercalation of H-atom to its bulk structure, chemically related to eq. 3, is the fundamental reaction in energy storage literature.[13]

$$H_2 + 2S \rightleftharpoons 2S\text{–H} \quad (1)$$

$$X + S\text{–H} \rightleftharpoons X\text{–H} + S \quad (2)$$

$$S + H^+ + e^- \rightleftharpoons S\text{–H} \quad (3)$$

$$2H^+ + 2e^- \rightleftharpoons H_2 \quad (4)$$

$$2H_2O \rightleftharpoons O_2 + 4H^+ + 4e^- \quad (5)$$

$$CO_2 + 2H^+ + 2e^- \rightleftharpoons CO + H_2O \quad (6)$$

$$N_2 + 6H^+ + 6e^- \rightleftharpoons 2NH_3 \quad (7)$$

Titanium dioxide (TiO_2) has long been known for its PCET reactivity. In 1972, Fujishima and Honda first discovered that TiO_2 can photoelectrochemically generate H_2 and O_2 from H_2O.[14] Classically, the TiO_2 reactivity has been described using the electronic band structure.[15,16] Formally a wide bandgap semiconductor, photoexcitation of TiO_2 under UV irradiation generates an electron-hole pair where the excited electrons are the source of reducing equivalences needed for the reduction of H_2O to H_2. The 'hole' remaining can serve as an oxidant to generate O_2 from H_2O.[17]

More recently, this model has been elaborated to incorporate the energetics of protons in overall reaction thermodynamics.[4,18-21] The catalytic activity towards H_2O splitting suggests that the surface sites undergo PCET reactions with the same number of protons and electrons, as evident from eqs. 4 and 5. For binary materials like TiO_2, the inner sphere PCET reaction with equimolar protons/electrons is thermochemically equivalent to a homolytic O–H bond formation and cleavage.[7] This thermochemical equivalence is illustrated using eqs. 8-10, involving a generic metal oxide, $M^{n+}O_x$. Thus, the O–H bond dissociation free energy (BDFE) that inherently integrates the thermodynamics of

electrons and protons can be considered a representative descriptor for an H-atom transfer reaction.[11] BDFEs are thermochemically related to the more general H-atom binding energy ($\Delta G°_H$) that is commonly referred to as the descriptor in catalysis literature as it *scales* with the activity (the Sabatier Principle).[3]

$$M^{n+}O_x + H^+ + e^- \rightleftharpoons M^{(n-1)+}O_{x-1}(OH) \quad (8)$$

$$H\cdot \rightleftharpoons H^+ + e^- \quad (9)$$

$$M^{n+}O_x + H\cdot \rightleftharpoons M^{(n-1)+}O_{x-1}(OH) \quad (10)$$

H-atom transfer thermochemistry of binary materials is highly dependent on their synthesis, morphologies, lattice structure, chemical history, and many others.[11,20,22-24] Surfaces of TiO_2 and many other metal oxides present multiple sites that can bind to H-atom(s) and are dynamically evolving when in contact with the reaction medium.[25-27] Chemically identical adsorption sites can laterally interact with each other to alter BDFEs.[11,28,29] H-atom intercalation within its lattice can cause the subsequent intercalation to be energetically favorable or unfavorable.[30,31] The structural ambiguity and heterogeneity between each H-atom adsorption site, and between each sample preclude fundamental understanding behind such stark differences in the *exact chemistry of H-atom transfer reactions*.

To attain structural precision and uniformity that enables atomic-level structural understanding of a reaction that further facilitates the integration of experimental and computational efforts, chemists have turned to metal–organic frameworks (MOFs) as candidate materials for the past few decades.[32-34] Particularly attractive amongst all MOFs are those with redox-active inorganic nodes dispersed throughout their porous structures that can undergo PCET reactions. This includes the MOF focused on this work, Ti-MIL-125 (Figure 1).[35,36] The Ti-oxo-based nodes ($Ti_8(\mu_2\text{-}O)_8(\mu_2\text{-}OH)_4$) separated by terephthalate linkers are known to undergo PCET reactions with equimolar amounts of protons and electrons, *i.e.,* the nodes undergo net H-atom transfer reactions. Through chemical titrations, the $Ti^{3+}O$–H BDFE was estimated to be <75 kcal mol^{-1}, but to the best of our understanding, the exact value is yet to be determined.[37] Quantification of BDFEs using a series of cyclic voltammogram (CV) measurements has been proven successful for many metal oxides,[11,20,21,38-41] and recently by us for the Ce-based MOF, Ce-MOF-808.[42] The low electron mobility within many MOFs, however, often leads to diffusive/kinetic complications.[43,44] In fact, the CVs of Ti-MIL-125 were quite ill-defined, with no obvious Faradaic feature that can be ascribed to the $Ti^{4+/3+}$ redox, altogether precluding this approach (*vide infra*).

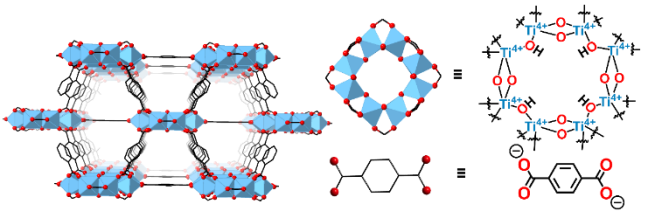

Figure 1. Structures of Ti-MIL-125, and its node and linker.

To this end, we employed open-circuit potential (E_{OCP}) measurement to *quantitatively* determine the $Ti^{3+}O$–H BDFE of Ti-MIL-125. Previously, E_{OCP} measurement has been applied to determine the equilibrium potentials of soluble and heterogenized redox couples in a given electrolyte.[41,45-48] In general, for a redox couple that undergoes mH$^+$/ne$^-$ PCET reaction (eq. 11), the E_{OCP} values with different concentrations of reduced (red) vs. oxidized (ox) species and proton activity (which is pH in an aqueous solution) should follow the Nernst equation (eq. 11). E_{OCP} measurements over these reaction conditions should construct the Pourbaix diagram, which can be used to extract the thermodynamic potential (E°).[49,50] Because each measurement is conducted under equilibrium conditions with no net current, kinetic/diffusive complications are minimal; thus E_{OCP}-derived BDFEs are generally more accurate than those using CVs.[45] This has proven a powerful tool to measure BDFEs of molecular species, including those that exhibit irreversible Faradaic features in CVs.[45] These encouraged our application to measure BDFEs using E_{OCP} by exploiting the long-term colloidal stability of nanosized Ti-MIL-125, reported by Brozek and co-workers.[51]

$$X + mH^+ + ne^- \rightleftharpoons XH_m^{(m-n)+} \quad (11)$$

$$E_{OCP} = E° - \frac{0.059}{n}\log\left(\frac{[red]}{[ox]}\right) - 0.059\left(\frac{m}{n}\right)pH \quad (12)$$

We demonstrate here the E_{OCP}-derived $Ti^{3+}O$–H BDFE of Ti-MIL-125 in a wide range of aqueous electrolytes. The determined BDFEs were further corroborated through the integration of computational calculations; these were eased due to the atomic-level structural understanding of the redox-active sites. To the best of our understanding, this represents the first report of E_{OCP}-derived thermochemistry of any MOF-based systems or colloidal suspension of redox-active species. The derived BDFEs are contrasted to those of other redox-active MOFs and metal oxides to highlight their implications in the catalysis field and beyond.

RESULTS

Ti-MIL-125 Synthesis and Electrochemical Measurements

Colloidally stable Ti-MIL-125 was synthesized using the modified procedure reported previously (see the Supporting Information (SI) for details).[51] The resulting MOF was characterized through N_2-adsorption-desorption isotherm and powder X-ray diffraction (PXRD) pattern. From the full-width-half-maximum (FWHM) of the PXRD patterns, the average particle size of Ti-MIL-125 was estimated to be *ca.* 15 nm; see Figures S1 and S2.

Ti-MIL-125 was suspended in neat methanol for photo-reduction under UV light, as reported previously.[37,51] The exact 'concentration' of Ti-MIL-125 has batch-to-batch differences (^{1}H NMR was used to estimate the concentration; see Figure S4). The use of the identical colloidal solution to prepare both the oxidized and reduced Ti-MIL-125 for each electrochemical measurement prevented any convolutions related to the concentration uncertainty; see the SI for details. Excessive photo-reduction can result in MOF degradation.[37] Indeed, with the reported nanosized Ti-MIL-125, reduction for 45 minutes under UV irradiation resulted in the maximum optical density, attributed to the presence of Ti^{3+}. A significant decrease in optical density was observed when the sample was further exposed to UV light (Figure S3). With an optimal photo-reduction, the

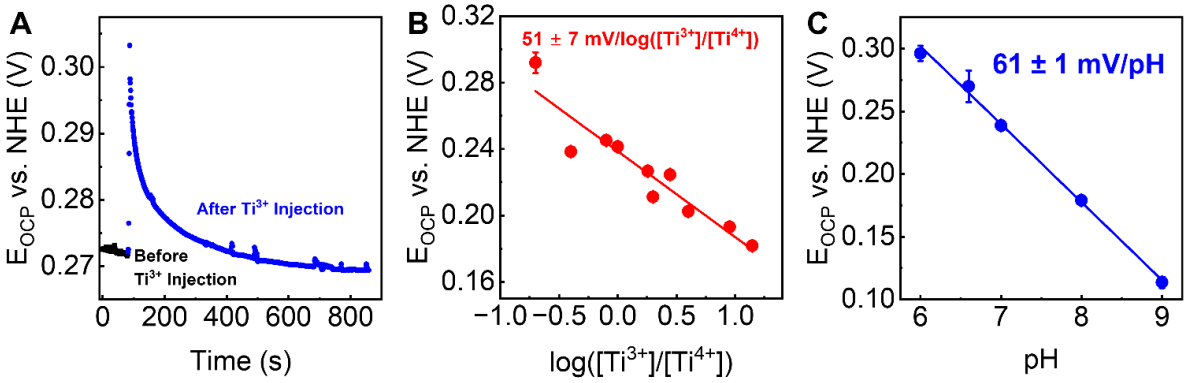

Figure 2. (**A**) Representative plot of E_{OCP} vs. normal hydrogen electrode (NHE) against reaction time in pH 7-adjusted Tris buffer. After 600 seconds, the E_{OCP} values stabilized; the average of the last 60 s was used for further analysis. The plot of E_{OCP} vs. NHE (**B**) against log([Ti^{3+}]/[Ti^{4+}]) and (**C**) against pH. (**B**) is a compilation of two separate measurements, with different concentrations of Ti^{3+} and Ti^{4+}; the error bars represent 1σ of E_{OCP} at the last 60 s or that of duplicate measurements, respectively. These errors are propagated in determining E°', which the errors from linear fits are shown as error bars in (**C**).

PXRD pattern of the reduced Ti^{3+}-MIL-125 was essentially identical to that of the oxidized Ti^{4+}-MIL-125 (Figure S2). The FWHM values of the two PXRD patterns were essentially identical. Together, these indicate that photoreduction did not result in ordered structural changes or deformation.

All electrochemical measurements were conducted under the N_2 atmosphere using the standard Schlenk line. Three aqueous buffers, 2-(N-morpholino) ethane sulfonic acid (MES), tris(hydroxymethyl)aminomethane (Tris), and boric acid, were adjusted to 100 mM concentration, unless otherwise noted, and their pH values were adjusted between 6 to 9. At all times, the electrochemical system was under N_2 atmosphere; aqueous electrolytes were degassed before any measurements by N_2 bubbling for at least 10 minutes. For most measurements, glassy carbon (GC) was used as the working electrode. CVs of colloidal Ti-MIL-125 resulted in an irreversible Faradaic feature (Figure S6), which precluded any accurate thermochemical analysis. E_{OCP} measurements instead were employed to determine the thermochemistry of the $Ti^{4+/3+}$ redox reaction, as described in the next sections.

Zeta-potential measurements revealed the non-linear trend in surface charges of colloidal Ti-MIL-125 with respect to the electrolyte pH (Figure S5). Implications of these surface charges in the PCET reactivity of Ti-MIL-125 are elaborated in the Discussion section.

E_{OCP} Measurement of Ti-MIL-125 in pH 7-Adjusted Aqueous Electrolyte

We begin this section with the E_{OCP} measurement of Ti-MIL-125 using pH 7-adjusted Tris buffer as a case study. Prior to the injection of photo-reduced Ti^{3+}-MIL-125, the electrolyte only contained the known amount of oxidized Ti^{4+}-MIL-125. The introduction of the photo-reduced Ti^{3+}-MIL-125 resulted in a cathodic shift in E_{OCP}; the measured potential equilibrated after 300-600 seconds, where the duration needed for equilibration seemingly depended on the amount of Ti^{4+} vs. Ti^{3+} in the electrolyte. Figure 2A is a representative plot showing how E_{OCP} changes as a function of time. After reaching equilibrium (*i.e.,* after ~600 s in Figure 2A), E_{OCP} varied less than 5 mV per minute, which corresponds to the change of <0.1 kcal mol^{-1} min^{-1}. The known volume of Ti^{3+}-MIL-125 was added to the electrolyte multiple times, which constantly led to a cathodic shift in E_{OCP} as a function of an increase in the nominal content of Ti^{3+} regardless of the initial electrolyte compositions (Figure 2B). The change in E_{OCP} with an increase in the 'concentration' of Ti^{3+} suggests that E_{OCP} is likely probing the equilibrium involving the Faradaic reaction near the electrode as described in eq. 12. For all concentrations, the average values of the last 60 seconds of measurements were used for further calculations. Our error analysis altering this range between 60 to 300 seconds indicates that the derived E_{OCP} values are largely independent of this time frame; see Figure S15 and the relevant section in the SI for details.

Over more than an order of magnitude of a change in Ti^{3+} vs. Ti^{4+} ratio, the measured E_{OCP} scaled in a single linear function with the slope of 51 mV per unit change in log([Ti^{3+}]/[Ti^{4+}]); see Figure 2B. According to the Nernst equation (eq. 12), this slope indicates that one electron is involved in the redox reaction.

The E_{OCP} measurements implicitly assume that (A) the working electrode surface is not directly participating in any inner-sphere electrochemical reactions and (B) formally redox-active species other than those of interest within the electrolyte are electrochemically innocent during the measurement. The first assumption was validated by measuring the E_{OCP} of an electrochemical cell with the same amount of reduced and oxidized Ti-MIL-125 using GC vs. gold electrode; see Figure S7. Regardless of the nature of the electrode, E_{OCP} values were identical.

Besides Ti-MIL-125, the electrolyte contains Tris and oxidized products of methanol, like formaldehyde; the latter is introduced during the injection of reduced Ti^{3+}-MIL-125. Both species can affect the E_{OCP} as they are redox-active.[52,53] Adding controlled amounts of 1 M Tris buffer while retaining the electrolyte pH at 7 resulted in minimal change in E_{OCP} (Figure S8). Thus, Tris buffers can be considered 'redox-innocent' in the reaction condition.

We have separately measured the role of methanol and formaldehyde by measuring E_{OCP} in pH 7-adjusted Tris

Scheme 1. Schematic illustration of $Ti^{3+}O–H$ BDFE Derivation

$$Ti_8^{4+}(\mu_2\text{-}O)_8(\mu_2\text{-}OH)_{4\,(s)} + nH^+_{(aq)} + ne^- \rightleftharpoons Ti_n^{3+}(\mu_2\text{-}OH)_n Ti_{8\text{-}n}^{4+}(\mu_2\text{-}O)_{8\text{-}n}(\mu_2\text{-}OH)_{4\,(s)} \qquad \Delta G^o/n = -FE^o \quad (14)$$

$$nH\bullet_{(aq)} \rightleftharpoons nH^+_{(aq)} + ne^- \qquad -C_G = -53 \text{ kcal mol}^{-1} \quad (15)$$

$$Ti_8^{4+}(\mu_2\text{-}O)_8(\mu_2\text{-}OH)_{4\,(s)} + nH\bullet_{(aq)} \rightleftharpoons Ti_n^{3+}(\mu_2\text{-}OH)_n Ti_{8\text{-}n}^{4+}(\mu_2\text{-}O)_{8\text{-}n}(\mu_2\text{-}OH)_{4\,(s)} \qquad \Delta G^o/n = -BDFE_{avg} \quad (16)$$

$$Ti^{3+}O\text{-}H\ BDFE_{avg} = 23.06\{E^o(Ti^{4+}O/Ti^{3+}O\text{-}H) \text{ vs. NHE}\} + C_G \quad (17)$$

buffer (with no colloidal MOFs). The addition of degassed methanol to this electrolyte led to no change in E_{OCP} (Figure S9). However, the subsequent addition of formaldehyde resulted in an anodic shift in E_{OCP} (Figure S10), which is expected from the Nernst equation (eq. 12) given that formaldehyde is an oxidized product of methanol.[45] This is quite distinct from the cathodic shift in E_{OCP} upon the introduction of reduced Ti^{3+}-MIL-125 to the electrolyte with some amount of Ti^{4+}-MIL-125. Thus, the E_{OCP} values described in Figures 2A and B are largely unperturbed by formaldehyde/methanol, perhaps due to their fast evaporation under constant N_2 bubbling.

Together, the E_{OCP} measurements were conducted over a wide range of $\log([Ti^{3+}]/[Ti^{4+}])$. The formal potential (E°') is defined when the concentrations of the reduced and oxidized species are equal, determined from the linear fit. In this case, the E°' vs. normal hydrogen electrode (NHE) of Ti-MIL-125 at pH 7 is 0.239 ± 0.004 V.

E_{OCP} Measurements of Ti-MIL-125 at Various Proton Activities and with Different Buffers

With the above measurements established, we have extended the E_{OCP} measurement in different aqueous buffers with pH ranging between 6 to 9. At all pHs, the slopes of E_{OCP} scaled roughly Nernstian with respect to the logarithm of the ratio, $[Ti^{3+}]/[Ti^{4+}]$, though sometimes the deviations were relatively large compared to that in Figure 2B; we note, however, that the measured slopes are still considered to be 'Nernstian' in the literature, including those using E_{OCP} of molecular species and soluble polyoxometalates (cf. [11,19,45,54]). The addition of methanol to the electrolyte may also obscure the proton activity, though as reported previously, this ambiguity was minimized by keeping the buffer concentration orders of magnitude higher than the redox-active species. We have conducted the error analysis associated with these complications in the SI to demonstrate that the associated errors are insignificant, particularly in deriving the thermochemistry of H-atom transfer, as detailed in the next section.

The observed slopes being *more-or-less* consistent with the expected 59 mV per $\log([Ti^{3+}]/[Ti^{4+}])$ suggest that in all pH values with distinct buffers, Ti-MIL-125 undergoes a redox reaction involving one electron.[55] As compared to those measured at pH 7 and 8, the run-to-run variations with different concentrations of Ti-MIL-125 were larger for those measurements at pH 6, 6.6, and 9 (see the SI for details). Notably, large variations were observed when the MOF crystallites had a negative surface charge, based on the zeta-potential measurements (Figures S11-14); implications of these two measurements are further elaborated in the Discussion section. E°' values determined at pH = 6 – 9 are listed in Table 1.

The derived E°' values scaled in a single linear function with respect to pH with a slope of 61 ± 1 mV/pH (Figure 2C). Fitting this value to the Nernst equation (eq. 12), the redox process involves an equal number of protons and electrons, and in this case, $1H^+/1e^-$. This stoichiometry is explicitly stated in the revised Nernst equation below (eq. 13). Here, we prefer to use 'concentrations' in the equation instead of surface coverages; while the latter is more common for Nernst equations of heterogenized, redox-active MOFs and metal oxides,[11,20,42] the use of concentration accurately reflects that the colloidal Ti-MIL-125 is treated as a 'homogeneous' species.

Table 1. E_{OCP} Measurement-Derived E°' values of Ti-MIL-125 at Various Buffers and pHs

pH	Buffer	E°' vs. NHE (V)[a]
6	MES	0.296(6)
6.6	MES	0.27(1)
7	Tris	0.239(4)
8	Tris	0.179(4)
9	Boric Acid	0.114(4)

[a]The errors of E°' values represent 1σ of linear regressions with different ratios of Ti^{3+} vs. Ti^{4+}; see the SI for details.

$$E_{OCP} = E° - 0.059 \log\left(\frac{[Ti^{3+}]}{[Ti^{4+}]}\right) - 0.059\ pH \quad (13)$$

E_{OCP}-Derived Free Energy of H-atom Transfer Reactions

With the proton-to-electron stoichiometry established, the standard potential (E°) derived from Figure 2C and the Nernst equation (eq. 13) can be applied to determine the free energy of the H-atom transfer reaction. Previous reports on PCET reactions using Ti-MIL-125 suggest that every node can accept *up to two H-atoms – i.e.,* in Scheme 1, $n = 1$ or 2. Dividing the total free energy of H-atom transfer by n gives the average $Ti^{3+}O–H$ BDFE.[7] The E° values were derived using two methods outlined previously;[42] first, the linear fit with 61 ± 1 mV/pH slope in Figure 2C was extrapolated to the standard state (pH = 0). Second, the slope of the linear fit was forced to be the ideal 59 mV/pH, and subsequently, E° values were derived from extrapolation.[42] The average of the two E° values are used here onwards (see the SI for more details).

As shown in Scheme 1, the free energy of nH^+/ne^- PCET reaction (eq. 14) and the homolytic cleavage of $Ti^{3+}O–H$ bond n times (eq. 16) are thermochemically equivalent, simply by using the formation free energy of H-atom (H·) from n number of proton and an electron; this has been determined to be 53 kcal mol^{-1} per nH^+/ne^- in H_2O and is often denoted as C_G (eq. 15).[7] Scheme 1 is essentially a derivation of the Bordwell equation (eq. 17), which was used

to derive the average $Ti^{3+}O–H$ BDFE to be 68 ± 2 kcal mol^{-1}. Because the nodes of Ti-MIL-125 have multiple sites at which $Ti^{3+}O–H$ bonds can form, and E_{OCP} solely reports the average BDFE, the proton topology of the nodes in Scheme 1 is not explicitly stated. The error analysis related to this BDFE value can be found in Figure S16 and the related sections in the SI.

Computational Calculations on H-atom Adsorbed, Ti_8 Nodes of Ti-MIL-125

To examine the proton topologies and the H-atom transfer thermochemistry of Ti-MIL-125 during the redox reaction, the PBE0 functional[56] and the def2-SVP basis set in Q-Chem 6.1 was employed to computationally model the structure.[57] The Ti_8 nodes were terminated with 12 formate linkers, following the standard procedure in the literature.[42,58] All structures were optimized using Baker's partitioned rational-function optimization (R-PFO)[59] and the self-consistent field (SCF) energy was converged to a cutoff of $1x10^{-6}$ a.u. using the geometric direct minimization algorithm (GDM).[60] Nodes with two added H-atoms were modelled in the triplet spin state. For all calculations, the enthalpic components were calculated and thus should technically be denoted bond dissociation enthalpy (BDE). We note, however, that for H-atom addition, entropic changes are minimal, and thus BDE is a good approximation for BDFE;[7] Our attempts to compute accurate BDFE with entropic components were unsuccessful with details and our speculations outlined in the Discussion section and the SI. The XYZ coordinates of the models can also be found in the SI.

First, we modelled the formate-terminated Ti_8 node with one extra H-atom; the proton was added to one μ_2–O, which mimics the previous reports (Figure 3A).[51] The spin density was localized on a single Ti cation adjacent to the μ_2–O(H), suggesting the reduction of that Ti^{4+} to Ti^{3+} (Figure S18). Compared to the fully oxidized node, an H-atom addition resulted in an increase in the Ti^{3+}–O(H) bond by 0.34 Å. The bond distance between the adjacent Ti^{4+} and the protonated μ_2–O(H) also increased by <0.1 Å. The computed $Ti^{3+}O–H$ BDE was ~62 kcal mol^{-1}, closely agreeing with the experimentally derived BDFE value. Because of the centro-symmetry of the Ti_8 nodes, the predicted BDE is independent of the position of Ti^{3+} and the adjacent μ_2–OH (which was originally μ_2–O).

The addition of one extra H-atom breaks the centro-symmetry of the Ti_8 node. Thus, the relative position of the second H-atom (*i.e.,* the spatial distribution of Ti^{3+} and a proton) with respect to the first must be considered. First, we considered the remaining μ_2–O groups as the Brønsted base sites. In this case, there are four proton topologies after two H-atom additions. Two of the four representative structures are shown in Figures 3B and C and the rest can be found in the SI. Similar to the first H-atom addition, this resulted in an increase in the Ti^{3+}–O(H) bond distance, ranging between 0.1 to 0.34 Å (see the SI for details), and the $Ti^{3+}O–H$ BDFE values were quite similar to the first BDFE, ranging between 61-63 kcal mol^{-1}. If instead the two protons are added to the same O-atom, resulting in μ_2–OH_2 (Figure 3D), the calculated BDFE was 41.0 kcal mol^{-1}, significantly deviating from the experimentally measured value. The Ti^{3+}–$O(H_2)$ bond distance increased by more than 0.6 Å. Together, these results suggest that each μ_2–O sites can accept only up to one proton during the PCET reaction.

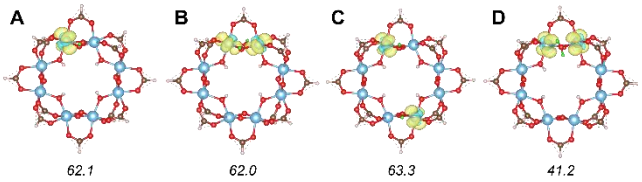

Figure 3. Computationally modelled Ti_8 nodes with (**A**) one H-atom, (**B-C**) two H-atoms with distinct proton topologies, and (**D**) μ_2–OH_2 between two Ti^{3+} cations. The calculated BDE values are shown under each node, in units of kcal mol^{-1}. Other proton topologies and bond distances can be found in the SI. Spin density colors: spin up = yellow, spin down = blue. Atom colors: added H-atoms = green, Ti = blue, O = red, C = brown, H = white.

DISCUSSION

Elaboration on Using E_{OCP} for Colloidal MOFs

Colloidally stable suspensions of Ti-MIL-125 in oxidized and photo-reduced states were prepared to measure the H-atom transfer thermochemistry on their Ti_8 nodes. CVs of colloidally suspended Ti-MIL-125 did not exhibit reversible Faradaic features; though estimations of thermochemistry can still be achieved with irreversible features,[61,62] its accuracy is far below that of using electrochemically reversible features. Instead, we turned to E_{OCP} measurements, in which the experimentally measured values were predictable by the Nernst equation (eq. 13).[45,46]

E_{OCP} measurements have been applied to determine the proton-to-electron stoichiometry and thermochemistry of molecular redox couples in aqueous and non-aqueous electrolytes.[45] In more recent years, this has been applied to polyoxovanadates.[41] In all cases, the reduced and oxidized species were completely soluble in the electrolyte. Thus, it was surprising that even for colloidal systems that are not formally solubilized, like the reported Ti-MIL-125, this method is still applicable. We note that the change in E_{OCP} of Ti-MIL-125 suspension in methanol-dimethylformamide (DMF) mixture upon photo-reduction has been reported previously,[51] though due to the lack of information on the proton activity, the measured E_{OCP} cannot be connected to the thermodynamics of the PCET reactions like those reported here.

The irreversible Faradaic feature in the CV of Ti-MIL-125 resembles those of molecular H-atom donors and acceptors with slow electron transfer kinetics. The redox reaction between (2,2,6,6-tetramethylpiperidin-1-yl)oxyl radical (TEMPO·) and its hydrogenated form, TEMPO-H, is the seminal example highlighting this phenomenon; even using the controlled potential electrolysis (CPE), the TEMPO-H formed via an electrochemical reduction of TEMPO· cannot be re-oxidized.[63,64] Thus, its O–H BDFE was instead measured using E_{OCP}.[45] The sluggish electron transfer should impact even further for colloidal crystallites like Ti-MIL-125. In fact, in general, CVs of nanoparticles (NPs) and other colloidally suspended substrates are often quasi-reversible, or totally irreversible. On top of slow electron

transfer kinetics, their diffusion to the electrode surface is slow, leading to CVs being 'non-ideal' for thermochemical analysis.[65-67]

Complications due to the slow diffusion of buffers and other electrolytes within the pores of MOFs often obscure the measured thermodynamics.[7] CVs of MOF-based electrodes typically exhibit large peak-to-peak separations (ΔE_p). This raises questions about the accuracy of the derived half-wave potential ($E_{½}$) needed for the Pourbaix diagram and the H-atom transfer thermodynamics.[68-70] We have previously employed Ce-MOF-808 and measured CVs over a wide pH range to determine the H-atom transfer thermochemistry. While this has proven successful, the standard errors of the linear fits used in the Pourbaix diagram were inevitably larger than those reported here.[42] In E_{OCP} measurements, these complications are nearly absent due to the longer experimental timescale allowing the system to reach equilibrium for every single reaction condition.[45,46] We will later return to the limitations of E_{OCP} measurements specific to Ti-MIL-125 and other MOFs.

This report demonstrates the feasibility of measuring the E_{OCP} of colloidal MOFs. Even though they are not 'homogeneous,' they can be treated much like soluble species. This enabled the determination of proton-to-electron stoichiometry and the associated H-atom transfer thermochemistry as described below.

PCET Reaction Mechanism of Ti-MIL-125

The E_{OCP} values of electrolytes containing reduced and oxidized Ti-MIL-125 scaled in a roughly Nernstian fashion with a unit change in $\log([Ti^{3+}]/[Ti^{4+}])$ and pH. Together, these established the proton-to-electron stoichiometry in the redox reaction to be 1:1.[55]

Within the pH range of 6–9, three buffers with distinct protic groups were deliberately chosen to examine their roles in the E_{OCP} measurement. The E°' values at various pHs all scaled in a single linear function with each data point deviating <5 mV (or <0.1 kcal mol^{-1}) from the linear fit (Figure 2C). This is strong evidence that the buffers within the electrolytes are simply acting as proton donors and acceptors with no *explicit role* in the PCET reaction. While we recently observed similar buffer independence in the H-atom transfer thermochemistry of Ce-MOF-808,[42] we emphasize that this is rarely observed for metal oxides and other binary materials. Nickel and cobalt-layered double hydroxides (LDHs) are well-known to have buffer-dependent $E_{½}$ values at the same pH, suggesting that buffers play an active role in the PCET reaction. In fact, strongly coordinating buffers like borate and phosphate anions have explicit roles in nickel/cobalt oxide-catalyzed, $4H^+/4e^-$ oxidation of H_2O to O_2.[22-24] Even for TiO_2, Fortunato *et al.* reported a drastic change in the Faradaic features of layered hydrogen titanate in the presence of phosphate vs. sulfate anions.[20] Compared to the bulk metal oxides, Ti-MIL-125 has relatively lower chemical stability, which precluded measurements in these acidic electrolytes with highly coordinating anions.[71,72] Still, we expect buffers like borate anions will interact much stronger than MES with weakly coordinating sulfonate groups. The independence of E_{OCP} with respect to the buffer concentration and the identity of the electrode (GC vs. Au) further highlights that the measured E_{OCP} is probing the $1H^+/1e^-$ PCET reactions on the nodes of Ti-MIL-125.

The observed Nernstian dependence of E_{OCP} vs. pH can be explained by (A) Ti_8 nodes undergoing the inner-sphere $1H^+/1e^-$ PCET reaction or (B) difference in electron transfer thermodynamics that is strongly correlated with surface charges due to protonation/deprotonation; Scheme 2 illustrates these two mechanisms using part of the Ti_8 node with one H-atom adsorbed for simplicity. Change in surface charge due to (de)protonation has been the common explanation of why band energies of semiconductors like Si or GaP with a thin layer of surface SiO_2/$GaPO_x$ exhibit a Nernstian dependence with respect to pH. The surface acidic groups such as SiO–H/GaPO–H protonate or deprotonate, and their surface populations are dependent on the difference between the electrolyte pH and their pK_a values. Hence, electron transfer to a de-protonated surface, for example, is less favorable due to a negative charge; in Scheme 2B, that would be the bottom reaction.[73,74] While E_{OCP} scaled in a single linear function with respect to pH, zeta-potentials of the crystallites exhibited a complex, non-linear dependence. The surface charges of Ti-MIL-125 were more negative in MES and borate buffer, *i.e.,* those that are anionic upon deprotonation. These stark differences in E_{OCP}/zeta-potential vs. pH trends suggest that the observed change in E_{OCP} is *not* due to surface charging/discharging.[18] The previously measured pK_a of Ti-MIL-125 also lies well outside the employed pH range.[75] Thus, our experimental efforts corroborate the previous notion that the Ti_8 nodes undergo an inner-sphere PCET reaction leading to bond formation/cleavage of the Ti^{3+}O–H bond (labeled A in Scheme 2). This parallels many other reports examining the PCET reaction of TiO_2,[18,37,76] including the report by Hupp and co-workers; they demonstrated the conduction band energy of TiO_2 scaled in a Nernstian fashion over >26 orders of magnitude change in proton activity.[77] This simply cannot be explained by the surface (de)protonation mechanism.

Scheme 2. Schematic Illustration of (A) Homolytic O–H Bond Formation of (B) O–H Group De-protonation on the Ti_8 Nodes of Ti-MIL-125

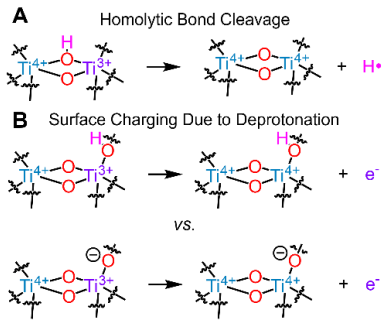

Each node of Ti-MIL-125 has been reported to accept up to $2H^+/2e^-$ (or two H-atoms).[37,51] If both H-atoms are transferred in the redox reaction, we expect E_{OCP} values to shift by 30 mV per unit change in $\log([Ti^{3+}]/[Ti^{4+}])$,[55] which contradicts the experimental observations. Our computational calculations have suggested that the first and the second H-atoms are bound to the Ti_8 nodes with very similar binding energies (*vide infra*). These suggest that Ti-MIL-125 with

one or two H-atoms can donate just one H-atom to a fully oxidized Ti-MIL-125 like those outlined in Schemes 3A and B. At the same time, nodes with one and two H-atoms can undergo an H-atom transfer reaction with each other, and the free energy of this reaction should be nearly thermoneutral; see Scheme 3C. We note that reactions illustrated in Schemes 3A and C are essentially a self-exchange reaction, involving H-atom transfer. All three reactions in Scheme 3 involve two distinct nodes, labeled Nodes 1 and 2; these nodes can be within one or multiple crystallites, and H-atoms can migrate between nodes through the mechanism speculated previously.[37] In all cases, the total number of protons/electrons involved in the reaction is one, agreeing with the experimentally observed value.

Scheme 3. Schematic Illustration of Three Possible PCET Reactions within Ti-MIL-125-Containing Electrolyte[a]

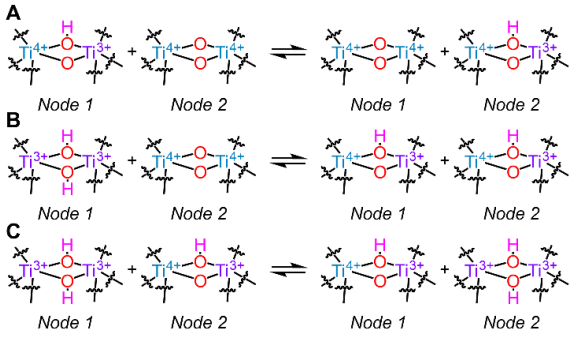

[a]In B and C, we used one of many proton topologies of Ti_8 nodes with two H-atoms; because $Ti^{3+}O–H$ BDFE of the second H-atom was very similar as long as the protonation upon the PCET reaction occurs at $\mu_2–O$, this scheme should hold for all proton topologies shown in Figures 3 and S18.

E_{OCP}-Derived $Ti^{3+}O–H$ BDFE of Ti-MIL-125 and Comparisons with Other Literature Values

The Pourbaix diagram plotting E°' of $Ti^{4+/3+}$ redox vs. pH (Figure 2C) was used to determine the average $Ti^{3+}O–H$ BDFE of Ti-MIL-125 to be 68 ± 2 kcal mol^{-1}. *To the best of our understanding, this is the first report on using E_{OCP} to derive any thermochemical value of MOFs.*

The BDFE measurements reported here were minimally hindered by the presence of other redox-active species which can otherwise obscure the values. As noted in the Results section, an increase in the concentration of redox-active Tris buffer resulted in minimal change in E_{OCP}. On the other hand, the addition of formaldehyde solution into methanol-containing pH 7-adjusted Tris buffer did result in a drastic change in E_{OCP}, but in an *anodic* direction. Formaldehyde is inevitably introduced during the addition of Ti^{3+} as it is the oxidized product of methanol. This anodic shift is expected from the Nernst equation (eq. 11) and if the observed E_{OCP} values were 'dominated' by the presence of formaldehyde, the E_{OCP} upon injection of Ti^{3+} suspension into the mixture of $Ti^{4+/3+}$-containing electrolytes should also shift anodically. Instead, at all MOF concentrations and buffers, we constantly observed a *cathodic* shift. The measured BDFE value significantly deviates from the average BDFE of the C/O–H bonds of methanol cleaved during the oxidation,[7] or the individual BDFEs estimated from BDEs;[78,79] in both cases, the differences in free energy are at least >30 kcal mol^{-1} (or >1.3 V). Thus, we conclude that the observed E_{OCP} values are instead probing the H-atom transfer thermochemistry of the Ti_8 nodes of Ti-MIL-125.

The measured $Ti^{3+}O–H$ BDFE agrees with the previously reported reactivity of reduced Ti^{3+}-MIL-125 towards 2,4,6-tri-t-butylphenoxyl radical (2,4,6-t-Bu-BuO·).[37] 2,4,6-tri-t-butylphenol (2,4,6-t-Bu-BuOH) has an O–H BDFE of 75 kcal mol^{-1}, and thus the H-atom transfer from the reduced Ti^{3+}-MIL-125 to 2,4,6-t-Bu-BuO· is a thermodynamically downhill reaction by *ca.* 8 kcal mol^{-1}.[7] The same report mentions the similar reactivity between reduced Ti^{3+}-MIL-125 and TEMPO·, apparent from the color change of MOF crystals.[37] Given that TEMPO–H has a BDFE similar to the value we determined for Ti-MIL-125 of 66 kcal mol^{-1},[7] this seemingly complete reactivity disagrees with our measurements. We note, however, that for TEMPO·, the reactivity study was convoluted due to its ready diffusion into the lattice as its molecular size is well below the pores of Ti-MIL-125. This convolution was absent for sterically bulky 2,4,6-t-Bu-BuOH. 'H-atom migration' from the bulk of the crystals to the surface has been observed for Ti-MIL-125, where the necessary protons are transferred between nodes through protic solvents like H_2O;[37,80] this may suggest that there is a driving force for bulk H-atoms to migrate to the surface – *i.e.,* at least the *apparent* $Ti^{3+}O–H$ BDFE is higher at the surface than in bulk. In the E_{OCP} measurements, the reduced and oxidized Ti-MIL-125 crystallites can exchange H-atoms, but only to Ti_8 nodes at the surfaces. Thus, E_{OCP} may be more sensitive to surface $Ti^{3+}O–H$ BDFE. The kinetics and fundamental reason for such bulk-to-surface H-atom migration is convoluted and thus, we prefer to focus on thermodynamics. Nevertheless, the $Ti^{3+}O–H$ BDFE measured here infers that there may be a thermodynamic reason behind this migration.

Mancuso *et al.* previously determined the steady-state potential of $Ti^{4+/3+}$ through spectroscopic observation of ferrocene (Fc) and ferrocenium (Fc^+) in acetonitrile (MeCN), using ethanol (EtOH) as a proton donor.[81] Fc^+ and ethanol were introduced to Ti^{3+}-MIL-125 to measure the Fc/Fc^+ ratio under equilibrium. The $Ti^{4+/3+}$ redox potential was estimated to be roughly –0.59 V vs. $Fc^{+/0}$, which was claimed to be just +36 mV more anodic of the $2H^+/H_2$ couple. This disagrees with our $Ti^{3+}O–H$ BDFE measurements being >10 kcal mol^{-1} (or >0.4 V) higher than the H–H BDFE of roughly 52 kcal mol^{-1}.[7] We speculate three reasons for this discrepancy. First, it must be noted that the reaction conditions between the above report and our E_{OCP} measurements are vastly different, and the two batches of Ti-MIL-125 were synthesized in a distinct manner. We cannot rule out differences arising from different reaction conditions. Nevertheless, mathematical conversion between E vs. $Fc^{+/0}$ to vs. $2H^+/H_2$ (which is NHE in aqueous electrolytes) simply using a 'constant' value has been highly discouraged for accurate thermochemical analysis (cf. [29,82,83]). This value to convert between the two reference potentials ranges between 0.53 to 0.64 V vs. NHE.[83-88] Furthermore, the exact proton activity in the MeCN/EtOH mixture is unknown and this uncertainty has been suggested as the potential source of error by Mancuso *et al.*[81] Below, we elabo-

rate on this through error analysis to rationalize the apparent differences in the measured $Ti^{3+}O–H$ BDFE.

Scheme 4 illustrates the thermochemical conversion of the PCET reaction in the MeCN/EtOH mixture (eq. 18) to homolytic O–H bond formation (eq. 16'). For simplicity, only the 'Ti–O' moiety within the node and one H-atom are considered. The O–H bond formation reaction in MeCN is closely related to that in H_2O, and hence are denoted as eqs. 16' and 16 in Schemes 4 and 2, respectively.[7,11,89] The pK_a of EtOH in MeCN is not reported but is expected to be above that of phenol (which is ~27).[90] Using the reported empirical method that converts the pK_a in H_2O to that in MeCN, the pK_a of EtOH in MeCN was calculated to be ~29;[91] this value was used in Scheme 4. We note that this is still an estimation of the 'true' proton activity. In aprotic solvents, acids and bases can undergo homo-conjugation.[92]

The resulting estimated $Ti^{3+}O–H$ BDFE is ~79 kcal mol^{-1}; while we reframe from excessive, quantitative comparisons of this value to others given many estimations used here, it is clear that this value is well above the H–H BDFE of 52 kcal mol^{-1}.[7] If the $Ti^{3+}O–H$ BDFE is close to 52 kcal mol^{-1}, Scheme 4 suggests that the pK_a of EtOH has to be ~10. The thermodynamic potential of $2H^+/H_2$ vs. $Fc^{+/0}$ in MeCN is $-0.028(4) - 0.059 \times pK_a$ V.[45,46] In order for the $2H^+/H_2$ couple to be –0.55 V vs. $Fc^{+/0}$ (*i.e.,* –0.59 + 0.036 V) noted above,[81] the pK_a of EtOH again has to be ~9. Regardless of the two methods, it is unlikely that the pK_a of EtOH is comparable to strong acids like HCl or p-toluenesulfonic acid with pK_a of 10 and 8.5, respectively.[90] Homoconjugations and other artifacts should not lead to ~20 pK_a unit differences. Significant errors in thermochemical calculations due to the lack of knowledge of proton activity have been reported multiple times in the literature (cf. [29,46,82]).

Scheme 4. Schematic Illustration of $Ti^{3+}O–H$ BDFE Derivation in MeCN/EtOH Mixture

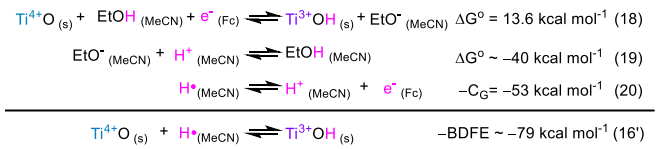

The above error analysis highlights the advantages of using E_{OCP} instead to measure H-atom thermochemistry. All E_{OCP} measurements were conducted with known proton activity and the amounts of Ti^{3+} vs. Ti^{4+}, and the measured E_{OCP} were all predictable by the Nernst equation (eq. 13). We argue here that much like how E_{OCP}-derived BDFEs are preferred for molecular species due to their enhanced quantitative accuracy,[45] E_{OCP} should be the preferred method to determine the H-atom transfer thermochemistry of colloidal MOFs.

Computational Corroboration of Ti_8 Node Structural Changes upon Redox Reaction

$Ti^{3+}O–H$ BDFE derived from E_{OCP} measurements and *in-silico* simulations were quantitatively similar, with a small difference of up to 7 kcal mol^{-1}. This slight disagreement may be due to the entropic component that is not considered in the computational model. Our attempts to compute entropic components were largely impeded by the arbitrarily high translational entropy of an isolated H-atom *in vacuo* prior to its binding to the Ti_8 node. Because in the actual experiment, the H-atoms are bound to the node and are exchanged, this entropic component does not reflect the *actual chemistry*. Computed BDE values were still quantitatively close to the experimental BDFE value following our previous success in computing BDE of Ce-MOF-808.[42]

Localization of spin densities regardless of the number of H-atoms or the node proton topologies parallels previous reports on H-atom addition to Ti-MIL-125 and TiO_2. Fabrizio *et al.* reported a similar localization of H-atoms using the Vienna *ab initio* Simulation Package (VASP).[51,93-95] The migration of H-atoms at the surface or bulk of TiO_2 is kinetically slow – in other words, the H^+/e^- are not delocalized (see below for more details).[96,97] Our computational efforts have further elucidated that while $Ti^{3+}–O$ bonds within the eight-membered ring changed up to 0.34 Å, the $Ti^{3+}–O$(linker) bonds were minimally altered even upon two H-atom addition; this suggests that the terephthalate linkers are minimally congested. The PXRD patterns of oxidized and photo-reduced Ti-MIL-125 were identical, corroborating the preservation of bulk MOF topology.

Overall, the close agreement between electrochemical and *in-silico* calculations proves the presented work to be accurately probing the H-atom transfer thermochemistry of Ti-MIL-125.

Comparisons of H-atom Transfer Thermochemistry between Ti-MIL-125 and TiO_2

The computational calculations of Ti_8 nodes have alluded that the measured $Ti^{3+}O–H$ BDFE of *ca.* 68 kcal mol^{-1} is likely probing the thermochemistry of both the first and second H-atoms adsorbed on the Ti_8 node, as long as $\mu_2–O$ serves as the Brønsted base. The above independence of BDFE to the number of adjacent H-atoms essentially suggests that the adsorbed H-atom follows the *ideal* Langmuir isotherm. In other words, the adsorbed H-atoms do not laterally interact with each other to alter their BDFEs.[98,99]

We speculate such H-atom coverage independence to relatively small changes to the ionic radii of Ti cation upon reduction and their interactions with carboxylates. Ti^{3+} cations are less than 0.1 Å larger than Ti^{4+}.[100] The $Ti^{3+}O–H$ BDFE of citrate-capped vs. uncapped TiO_2 NPs are quantitatively identical, suggesting that Ti-carboxylate interactions have minimal effect on H-atom transfer reactions.[18] As noted above, the bond distance changes were quite localized near Ti^{3+} cations even after two H-atom additions, and thus lattice strain-induced BDFE distribution is unlikely. Indeed, for all proton topologies we examined computationally, the $Ti^{3+}–O$(linker) bond changed by less than 0.1 Å. The band energies upon redox reactions have been demonstrated to be independent of the number of H-atoms per node by Mancuso *et al.*, which supports our observation;[81] we note, however, that their absolute BDFE value estimated from the calculated band energies contradicts our report and we discussed the reasons for this difference above.

To the best of our knowledge, amongst all heterogeneous systems with Ti-oxo moieties, TiO_2 NP is the only material that exhibits the Langmuir isotherm.[18] Even at reasonably high H-atom coverage with up to one H-atom per 10 Ti cations, the $Ti^{3+}O–H$ BDFE values were *more similar than*

different.[18] Compared to TiO_2 NPs, bulk TiO_2 can often exhibit a wide range of BDFE. Balland and co-workers have shown that amorphous TiO_2 exhibits > 10 kcal mol^{-1} width in BDFE distribution.[30] On the other hand, anatase TiO_2 exhibits a distribution narrower than the ideal Langmuir isotherm, suggesting that H-atom adsorption (and insertion) are thermodynamically more favorable when anatase TiO_2 *already has H-atoms*. In the *Semiconductor Electrodes,* Finklea has demonstrated that the flat-band potentials of TiO_2 can have ~0.5 eV (or >10 kcal mol^{-1}) deviations from each other at a given pH, depending on the synthetic protocol and chemical history.[101] This surface-coverage-dependent BDFE has been ascribed to lateral interactions between adsorbates and/or chemical heterogeneity, combined most likely in a complex manner.[98,102,103]

Implications of $Ti^{3+}O$–H BDFE on Reactions of H_2

Under UV irradiation, TiO_2 evolves H_2 from H_2O, but only after a certain irradiation period.[27,104] This induction period has been classically ascribed to the kinetic reason. H-atoms on the surface of TiO_2 have O–H BDFEs typically ranging between 40 to 49 kcal mol^{-1}.[7,12,18] Thus, H_2 formation should be thermodynamically downhill. However, the slow diffusion of these H-atoms through the lattice prevents the release of H_2.[96,97]

The Ti^{3+}O–H BDFE of Ti-MIL-125 is well above that of H_2 regardless of the number of H-atoms per node as long as μ_2–O is protonated – in other words, for Ti-MIL-125, the H_2 evolution reaction (HER) is thermodynamically uphill. Perhaps, this explains why co-catalysts (*e.g.,* Pt NPs) are commonly employed in many reports of Ti-MIL-125-catalyzed H_2 evolution reaction (HER), where in these cases the MOF simply acts as a photosensitizer.[105-107] This relatively high Ti^{3+}O–H BDFE is tentatively ascribed to the rather unique ring-like structure of Ti_8 nodes that are 'locked' within the MOF network. If similar Ti-oxo moieties exist on surfaces of TiO_2, this can explain the observed induction period in TiO_2-catalyzed HER; H-atoms adsorbed at the initial stage of the reaction are on these moieties and are *not* released as H_2. HER only happens at other distinct sites with significantly weaker Ti^{3+}O–H BDFE. As noted above, the surfaces of TiO_2 are known to undergo a dynamic structural transformation during HER,[27] and thus, it is experimentally challenging to probe the presence of a Ti_8 node-like structure on the TiO_2 surface. Our measurements simply infer an alternative *thermodynamic* explanation behind the observed induction period in TiO_2-catalyzed HER. In practice, it is likely that kinetic, thermodynamic, and perhaps other reasons have complex contributions.

The reported findings on the thermochemistry of Ti-MIL-125 cannot determine the exact reason behind the differences in BDFEs of Ti-MIL-125 and TiO_2. These remain a fundamental challenge in the field of surface science and electrocatalysis, even for crystalline materials like MOFs.[11,28,29,108] Nevertheless, our electrochemical and computational efforts on Ti-MIL-125 suggest that the Ti_8 node is a stronger H-atom acceptor than TiO_2 even though locally, their compositions are similar.

Limitations in E_{OCP} Measurements of Ti-MIL-125

While E_{OCP} measurements have proven successful in the reported buffers and pH, many attempts beyond the reported reaction conditions led to MOF decomposition. In general, Ti-based MOFs have lower chemical stability than MOFs with the other Group IV transition metal cations, *i.e,* Zr- and Hf-based MOFs;[72] the latter two are largely redox-innocent, so without functionalization, their MOFs are electrochemically inert.[44] The lack of suitable and stable buffers also precluded exploration beyond the reported pH range. We have attempted to use acetic acid/acetate buffer for the pH range of 4–5, but instead led to an immediate decomposition of Ti-MIL-125; this is likely due to the displacement of terephthalate linkers by acetate anions. This attempt was largely prompted because of the reported pK_a of Ti-MIL-125 being ~4.5.[75] The buffer concentration must be orders of magnitude higher than that of Ti-MIL-125 for accurate E_{OCP} measurements, which precludes the dilution of buffers.[45] In general, there lacks a buffer at pH <5, which does not strongly coordinate to Ti_8 nodes to prevent MOF decomposition.

The sample-to-sample variation was seemingly dependent on the zeta-potential of the Ti-MIL-125 crystallites in the buffer. At pH 6, 6.6, and 9, the zeta-potentials were highly negative, around –20 mV. While we are unsure of the exact role or reasoning behind such negative surface charges, it is conceivable that this can decrease the electron transfer reactions between crystallites during the equilibration, which are known to hinder electrochemical measurements (see above). The previous report on using E_{OCP} to determine BDFEs of non-polar C–H bonds using molecules like anthracene/dihydroanthracene was proven unsuccessful, also due to the slow electron transfer kinetics. In fact, tetrahydrofuran (THF) was used as a solvent for many molecular species, indicating that its $4H^+/4e^-$ oxidation to furan involving two C–H bond cleavages is not perturbing the E_{OCP} measurements.[45] This parallels the apparent electrochemical inertness of Tris buffer in our work. Even for more polar O–H bonds, redox couples like 2,4,6-t-Bu-BuOH/2,4,6-t-Bu-BuO· had significantly high sample-to-sample/day-to-day variation and many times, the linear fits had slopes quite distinct from the ideal 59 mV per log([red]/[ox]); this is qualitatively similar to our observations at pH 6 and 6.6.[45] This inconsistency is reported to be even more pronounced for polyoxovanadates.[41] The kinetics of (proton-coupled) electron transfer between two colloidal MOF crystallites must be slower than molecular species or polyoxometalates. Thus, this explanation seems to agree with the batch-to-batch dependence and some deviations from the Nernstian slope observed in some of the buffers in this report. We note, however, that even if E°' derived from these 'less ideal' measurements were removed, the linear fit in the Pourbaix diagram and the derived Ti^{3+}O–H BDFE is minimally altered, and thus the conclusions stated here are not dependent on these limitations.

We acknowledge many challenges associated with E_{OCP} measurements of MOFs. The reported success in deriving Ti^{3+}O–H BDFE, however, should still prove as powerful evidence that this technique can be applied for accurate BDFE measurements of colloidal MOFs, and perhaps other colloidal systems with limited methods for accurate thermochemical analysis.

CONCLUSIONS AND FUTURE OUTLOOK

H-atom binding energy on the Ti_8 nodes of the MOF, Ti-MIL-125 was experimentally determined using a series of E_{OCP} measurements. The colloidal stability of nanosized Ti-MIL-125 enabled E_{OCP} measurements, where the crystallites were treated as 'homogeneous' species. The experimentally derived free energy of H-atom transfer, $Ti^{3+}O–H$ BDFE, was more accurate than previously reported methods. The enhanced accuracy of calculated BDFE using E_{OCP} vs. other electrochemical/spectroscopic techniques has been elaborated for molecular species[45] and we argue this is true even for Ti-MIL-125.

Our BDFE measurements were corroborated using computational simulations. Atomically precise structural knowledge of the Ti_8 nodes ensured that the simulations were representative of the actual system. We emphasize that to the best of our understanding, this is the first report on using E_{OCP} to derive the thermochemistry of any MOF-based system. Given this success, it is tempting to claim that E_{OCP} measurements may be a viable method to measure the H-atom transfer thermochemistry of other colloidal systems beyond MOFs.

The experimentally derived $Ti^{3+}O–H$ BDFE of roughly 68 kcal mol^{-1} is larger by *ca.* 20 kcal mol^{-1} than those experimentally/computationally derived for bulk TiO_2.[18,76] We tentatively ascribe such stark differences in BDFEs to the somewhat unique Ti-oxo ring-like structure that cannot reorganize even after H-atom adsorption without MOF degradation. A similar structure may be present on TiO_2 surfaces, at least initially, but would likely evolve in its structure as more H-atoms get adsorbed. This structural evolution is minimized in Ti-MIL-125 as the node structure is critical to retaining the porous structure.

Whatever the reason for such a difference in BDFE is, we advocate that this drastic difference suggests that Ti-oxo moieties with similar *local* structures can have drastically different reactivity in H-atom transfer reactions. Unlike bulk TiO_2, Ti-MIL-125 has a >20 kcal mol^{-1} thermodynamic driving force to accept H-atoms; thus even though the two materials contain a similar structural motif, their reactivity in PCET/H-atom transfer reactions is quite distinct. These uniquely high BDFE values can be useful for chemical transformations involving H-atom transfer that TiO_2 cannot otherwise catalyze, and this is our current research focus. We are further exploring other Ti-based MOFs with distinct node structures and MOF topologies that may alter the BDFE. The presented work should become the cornerstone of the accurate determination of BDFEs of nanosized MOFs and other colloidal systems, which are critical to electrocatalyst design for renewable energy transformation and many others.

ASSOCIATED CONTENT

The supporting information is available free of charge at.

AUTHOR INFORMATION

Corresponding Author

* Hyunho Noh – Department of Chemistry and Biochemistry, University of Oklahoma, Norman OK 73019; orcid.org/0000-0003-3136-1004; Email: hyunho.noh-1@ou.edu

Notes

The authors declare no competing financial interest.

ACKNOWLEDGMENT

H.N. acknowledges the support from the University of Oklahoma startup funds. Y.S. is supported by the National Science Foundation via grant No. CHE-2102071. The computing for this project by N.G.A., C.W.L., and Y.S. was performed at the High Performance Computing Center at Oklahoma State University supported in part through the National Science Foundation grant OAC-1531128. Work by A.R. was supported by the Catalyst Design for Decarbonization Center, an Energy Frontier Research Center, which is funded by the US Department of Energy (DOE), Office of Science, Basic Energy Sciences (BES) under award DE-SC0023383. PXRD pattern collections were performed at the Samuel Roberts Noble Microscopy Laboratory, an OU core facility supported by the Vice President for Research and Partnerships. This work made use of the NUFAB facility of Northwestern University's NUANCE Center, which has received support from the SHyNE Resource (NSF ECCS-2025633), the IIN, and Northwestern's MRSEC program (NSF DMR-2308691). N.G.A. and H.N. acknowledge Dr. Preston R. Larson for his help in collecting the PXRD patterns using capillaries, Dr. Mansu Kim at Northwestern University for coordinating the zeta-potential measurements, and Dr. Daniel T. Glatzhofer for providing chemicals and the UV photo-reactor.

REFERENCES

1. Nocera, D. G., Proton-Coupled Electron Transfer: The Engine of Energy Conversion and Storage. *J. Am. Chem. Soc.* **2022,** *144* (3), 1069-1081.
2. Lewis, N. S.; Nocera, D. G., Powering the planet: Chemical challenges in solar energy utilization. *Proc. Natl. Acad. Sci. U. S. A.* **2006,** *103* (43), 15729-15735.
3. Seh, Z. W.; Kibsgaard, J.; Dickens, C. F.; Chorkendorff, I.; Nørskov, J. K.; Jaramillo, T. F., Combining theory and experiment in electrocatalysis: Insights into materials design. *Science* **2017,** *355* (6321), eaad4998.
4. Mayer, J. M., Bonds over Electrons: Proton Coupled Electron Transfer at Solid–Solution Interfaces. *J. Am. Chem. Soc.* **2023,** *145* (13), 7050-7064.
5. Murray, P. R. D.; Cox, J. H.; Chiappini, N. D.; Roos, C. B.; McLoughlin, E. A.; Hejna, B. G.; Nguyen, S. T.; Ripberger, H. H.; Ganley, J. M.; Tsui, E.; Shin, N. Y.; Koronkiewicz, B.; Qiu, G.; Knowles, R. R., Photochemical and Electrochemical Applications of Proton-Coupled Electron Transfer in Organic Synthesis. *Chem. Rev.* **2022,** *122* (2), 2017-2291.
6. Bard, A. J., Inner-Sphere Heterogeneous Electrode Reactions. Electrocatalysis and Photocatalysis: The Challenge. *J. Am. Chem. Soc.* **2010,** *132* (22), 7559-7567.
7. Agarwal, R. G.; Coste, S. C.; Groff, B. D.; Heuer, A. M.; Noh, H.; Parada, G. A.; Wise, C. F.; Nichols, E. M.; Warren, J. J.; Mayer, J. M., Free Energies of Proton-Coupled Electron Transfer Reagents and Their Applications. *Chem. Rev.* **2021,** *122* (1), 1-49.
8. Green, S. A.; Crossley, S. W. M.; Matos, J. L. M.; Vásquez-Céspedes, S.; Shevick, S. L.; Shenvi, R. A., The High Chemofidelity of Metal-Catalyzed Hydrogen Atom Transfer. *Acc. Chem. Res.* **2018,** *51* (11), 2628-2640.
9. Kamei, Y.; Seino, Y.; Yamaguchi, Y.; Yoshino, T.; Maeda, S.; Kojima, M.; Matsunaga, S., Silane- and peroxide-free hydrogen atom transfer hydrogenation using ascorbic acid and cobalt-photoredox dual catalysis. *Nat. Commun.* **2021,** *12* (1), 966.
10. Crossley, S. W. M.; Obradors, C.; Martinez, R. M.; Shenvi, R. A., Mn-, Fe-, and Co-Catalyzed Radical Hydrofunctionalizations of Olefins. *Chem. Rev.* **2016,** *116* (15), 8912-9000.
11. Noh, H.; Mayer, J. M., Medium-Independent Hydrogen Atom Binding Isotherms of Nickel Oxide Electrodes. *Chem* **2022,** *8* (12), 3324-3345.
12. Warburton, R. E.; Soudackov, A. V.; Hammes-Schiffer, S., Theoretical Modeling of Electrochemical Proton-Coupled Electron Transfer. *Chem. Rev.* **2022,** *122* (12), 10599-10650.
13. Augustyn, V.; Simon, P.; Dunn, B., Pseudocapacitive oxide materials for high-rate electrochemical energy storage. *Energy Environ. Sci.* **2014,** *7* (5), 1597-1614.

14. Fujishima, A.; Honda, K., Electrochemical Photolysis of Water at a Semiconductor Electrode. *Nature* **1972,** *238* (5358), 37-38.
15. Grätzel, M., Photoelectrochemical cells. *Nature* **2001,** *414* (6861), 338-344.
16. Gerischer, H.; Decker, F.; Scrosati, B., The Electronic and the Ionic Contribution to the Free Energy of Alkali Metals in Intercalation Compounds. *J. Electrochem. Soc.* **1994,** *141* (9), 2297.
17. Schneider, J.; Matsuoka, M.; Takeuchi, M.; Zhang, J.; Horiuchi, Y.; Anpo, M.; Bahnemann, D. W., Understanding TiO_2 Photocatalysis: Mechanisms and Materials. *Chem. Rev.* **2014,** *114* (19), 9919-9986.
18. Peper, J. L.; Gentry, N. E.; Boudy, B.; Mayer, J. M., Aqueous TiO_2 Nanoparticles React by Proton-Coupled Electron Transfer. *Inorg. Chem.* **2021,** *61* (2), 767-777.
19. Nedzbala, H. S.; Westbroek, D.; Margavio, H. R. M.; Yang, H.; Noh, H.; Magpantay, S. V.; Donley, C. L.; Kumbhar, A. S.; Parsons, G. N.; Mayer, J. M., Photoelectrochemical Proton-Coupled Electron Transfer of TiO_2 Thin Films on Silicon. *J. Am. Chem. Soc.* **2024,** *146* (15), 10559-10572.
20. Fortunato, J.; Shin, Y. K.; Spencer, M. A.; van Duin, A. C. T.; Augustyn, V., Choice of Electrolyte Impacts the Selectivity of Proton-Coupled Electrochemical Reactions on Hydrogen Titanate. *J. Phys. Chem. C* **2023,** *127* (25), 11810-11821.
21. Cooney, S. E.; Walls, M. R. A.; Schreiber, E.; Brennessel, W. W.; Matson, E. M., Heterometal Dopant Changes the Mechanism of Proton-Coupled Electron Transfer at the Polyoxovanadate-Alkoxide Surface. *J. Am. Chem. Soc.* **2024,** *146* (4), 2364-2369.
22. Surendranath, Y.; Dincă, M.; Nocera, D. G., Electrolyte-Dependent Electrosynthesis and Activity of Cobalt-Based Water Oxidation Catalysts. *J. Am. Chem. Soc.* **2009,** *131* (7), 2615-2620.
23. Dincă, M.; Surendranath, Y.; Nocera, D. G., Nickel-borate oxygen-evolving catalyst that functions under benign conditions. *Proc. Nat. Acad. Sci.* **2010,** *107* (23), 10337-10341.
24. Esswein, A. J.; Surendranath, Y.; Reece, S. Y.; Nocera, D. G., Highly active cobalt phosphate and borate based oxygen evolving catalysts operating in neutral and natural waters. *Energy Environ. Sci.* **2011,** *4* (2), 499-504.
25. Grimaud, A.; Demortière, A.; Saubanère, M.; Dachraoui, W.; Duchamp, M.; Doublet, M.-L.; Tarascon, J.-M., Activation of surface oxygen sites on an iridium-based model catalyst for the oxygen evolution reaction. *Nat. Energy* **2016,** *2* (1), 16189.
26. Akbashev, A. R.; Zhang, L.; Mefford, J. T.; Park, J.; Butz, B.; Luftman, H.; Chueh, W. C.; Vojvodic, A., Activation of ultrathin $SrTiO_3$ with subsurface $SrRuO_3$ for the oxygen evolution reaction. *Energy Environ. Sci.* **2018,** *11* (7), 1762-1769.
27. Lu, Y.; Yin, W.-J.; Peng, K.-L.; Wang, K.; Hu, Q.; Selloni, A.; Chen, F.-R.; Liu, L.-M.; Sui, M.-L., Self-hydrogenated shell promoting photocatalytic H_2 evolution on anatase TiO_2. *Nat. Commun.* **2018,** *9* (1), 2752.
28. Strmcnik, D.; Tripkovic, D.; van der Vliet, D.; Stamenkovic, V.; Marković, N. M., Adsorption of hydrogen on Pt(111) and Pt(100) surfaces and its role in the HOR. *Electrochem. Commun.* **2008,** *10* (10), 1602-1605.
29. Agarwal, R. G.; Kim, H.-J.; Mayer, J. M., Nanoparticle O–H Bond Dissociation Free Energies from Equilibrium Measurements of Cerium Oxide Colloids. *J. Am. Chem. Soc.* **2021,** *143* (7), 2896-2907.
30. Makivić, N.; Cho, J.-Y.; Harris, K. D.; Tarascon, J.-M.; Limoges, B.; Balland, V., Evidence of Bulk Proton Insertion in Nanostructured Anatase and Amorphous TiO_2 Electrodes. *Chem. Mater.* **2021,** *33* (9), 3436-3448.
31. Miu, E. V.; Mpourmpakis, G.; McKone, J. R., Predicting the Energetics of Hydrogen Intercalation in Metal Oxides Using Acid–Base Properties. *ACS Appl. Mater. Interfaces* **2020,** *12* (40), 44658-44670.
32. Wei, Y.-S.; Zhang, M.; Zou, R.; Xu, Q., Metal–Organic Framework-Based Catalysts with Single Metal Sites. *Chem. Rev.* **2020,** *120* (21), 12089-12174.
33. Bavykina, A.; Kolobov, N.; Khan, I. S.; Bau, J. A.; Ramirez, A.; Gascon, J., Metal–Organic Frameworks in Heterogeneous Catalysis: Recent Progress, New Trends, and Future Perspectives. *Chem. Rev.* **2020,** *120* (16), 8468-8535.
34. Liu, J.; Goetjen, T. A.; Wang, Q.; Knapp, J. G.; Wasson, M. C.; Yang, Y.; Syed, Z. H.; Delferro, M.; Notestein, J. M.; Farha, O. K.; Hupp, J. T., MOF-enabled confinement and related effects for chemical catalyst presentation and utilization. *Chem. Soc. Rev.* **2022,** *51* (3), 1045-1097.
35. Fu, Y.; Sun, D.; Chen, Y.; Huang, R.; Ding, Z.; Fu, X.; Li, Z., An Amine-Functionalized Titanium Metal–Organic Framework Photocatalyst with Visible-Light-Induced Activity for CO_2 Reduction. *Angew. Chem. Int. Ed.* **2012,** *51* (14), 3364-3367.
36. Dan-Hardi, M.; Serre, C.; Frot, T.; Rozes, L.; Maurin, G.; Sanchez, C.; Férey, G., A New Photoactive Crystalline Highly Porous Titanium(IV) Dicarboxylate. *J. Am. Chem. Soc.* **2009,** *131* (31), 10857-10859.
37. Saouma, C. T.; Richard, S.; Smolders, S.; Delley, M. F.; Ameloot, R.; Vermoortele, F.; De Vos, D. E.; Mayer, J. M., Bulk-to-Surface Proton-Coupled Electron Transfer Reactivity of the Metal–Organic Framework MIL-125. *J. Am. Chem. Soc.* **2018,** *140* (47), 16184-16189.
38. (a) Wise, C. F. M., J. M., Electrochemically Determined O–H Bond Dissociation Free Energies of NiO Electrodes Predict Proton-Coupled Electron Transfer Reactivity. *J. Am. Chem. Soc.* **2019,** *141* (38), 14971-14975. (b) Wise, C. F.; Mayer, J. M., Correction to "Electrochemically Determined O–H Bond Dissociation Free Energies of NiO Electrodes Predict Proton-Coupled Electron Transfer Reactivity". *J. Am. Chem. Soc.* **2020,** *142* (28), 12544-12545.
39. Samantaray, Y.; Martin, D. J.; Agarwal, R. G.; Gibson, N. J.; Mayer, J. M., Proton-Coupled Electron Transfer of Cerium Oxide Nanoparticle Thin-Film Electrodes. *J. Phys. Chem. C* **2023,** *127* (8), 4015-4020.
40. Schreiber, E.; Fertig, A. A.; Brennessel, W. W.; Matson, E. M., Oxygen-Atom Defect Formation in Polyoxovanadate Clusters via Proton-Coupled Electron Transfer. *J. Am. Chem. Soc.* **2022,** *144* (11), 5029-5041.
41. Proe, K. R.; Towarnicky, A.; Fertig, A.; Lu, Z.; Mpourmpakis, G.; Matson, E. M., Impact of Surface Ligand Identity and Density on the Thermodynamics of H Atom Uptake at Polyoxovanadate-Alkoxide Surfaces. *Inorg. Chem.* **2024,** *63* (16), 7206-7217.
42. Ingram, Z. J.; Lander, C. W.; Oliver, M. C.; Altınçekiç, N. G.; Huang, L.; Shao, Y.; Noh, H., Hydrogen-Atom Binding Energy of Structurally Well-defined Cerium Oxide Nodes at the Metal–Organic Framework-Liquid Interfaces. *J. Phys. Chem. C* **2024,** *128* (23), 9556–9565.
43. Xie, L. S.; Skorupskii, G.; Dincă, M., Electrically Conductive Metal–Organic Frameworks. *Chem. Rev.* **2020,** *120* (16), 8536-8580.
44. Kung, C.-W.; Goswami, S.; Hod, I.; Wang, T. C.; Duan, J.; Farha, O. K.; Hupp, J. T., Charge Transport in Zirconium-Based Metal–Organic Frameworks. *Acc. Chem. Res.* **2020,** *53* (6), 1187-1195.
45. Wise, C. F.; Agarwal, R. G.; Mayer, J. M., Determining Proton-Coupled Standard Potentials and X–H Bond Dissociation Free Energies in Nonaqueous Solvents Using Open-Circuit Potential Measurements. *J. Am. Chem. Soc.* **2020,** *142* (24), 10681-10691.
46. Roberts, J. A. S.; Bullock, R. M., Direct Determination of Equilibrium Potentials for Hydrogen Oxidation/Production by Open Circuit Potential Measurements in Acetonitrile. *Inorg. Chem.* **2013,** *52* (7), 3823-3835.
47. Kinoshita, K.; Madou, M. J., Electrochemical Measurements on Pt, Ir, and Ti Oxides as pH Probes. *J. Electrochem. Soc.* **1984,** *131* (5), 1089.
48. Ardizzone, S.; Carugati, A.; Trasatti, S., Properties of thermally prepared iridium dioxide electrodes. *J. Electroanal. Chem. Interfacial Electrochem.* **1981,** *126* (1), 287-292.
49. Pourbaix, M., *Atlas of Electrochemical Equilibria in Aqueous Solution*. Houston, TX, 1974.
50. Pourbaix, M., Thermodynamics and corrosion. *Corros. Sci.* **1990,** *30* (10), 963-988.
51. Fabrizio, K.; Gormley, E. L.; Davenport, A. M.; Hendon, C. H.; Brozek, C. K., Gram-scale synthesis of MIL-125 nanoparticles and their solution processability. *Chem. Sci.* **2023,** *14* (33), 8946-8955.
52. Lai, B.-C.; Wu, J.-G.; Luo, S.-C., Revisiting Background Signals and the Electrochemical Windows of Au, Pt, and GC Electrodes in Biological Buffers. *ACS Appl. Energy Mater.* **2019,** *2* (9), 6808-6816.
53. Hamnett, A., Mechanism and electrocatalysis in the direct methanol fuel cell. *Catal. Today* **1997,** *38* (4), 445-457.
54. Jackson, M. N.; Pegis, M. L.; Surendranath, Y., Graphite-Conjugated Acids Reveal a Molecular Framework for Proton-

Coupled Electron Transfer at Electrode Surfaces. *ACS Cent. Sci.* **2019,** *5* (5), 831-841.
55. Bard, A. J.; Faulkner, L. R., *Electrochemical Methods: Fundamentals and Applications*. John Wiley & Sons Inc.: New York, NY, 2001.
56. Perdew, J. P.; Burke, K.; Ernzerhof, M., Generalized Gradient Approximation Made Simple. *Phys. Rev. Lett.* **1996,** *77* (18), 3865-3868.
57. Epifanovsky, E.; Gilbert, A. T. B.; Feng, X.; Lee, J.; Mao, Y.; Mardirossian, N.; Pokhilko, P.; White, A. F.; Coons, M. P.; Dempwolff, A. L.; Gan, Z.; Hait, D.; Horn, P. R.; Jacobson, L. D.; Kaliman, I.; Kussmann, J.; Lange, A. W.; Lao, K. U.; Levine, D. S.; Liu, J.; McKenzie, S. C.; Morrison, A. F.; Nanda, K. D.; Plasser, F.; Rehn, D. R.; Vidal, M. L.; You, Z.-Q.; Zhu, Y.; Alam, B.; Albrecht, B. J.; Aldossary, A.; Alguire, E.; Andersen, J. H.; Athavale, V.; Barton, D.; Begam, K.; Behn, A.; Bellonzi, N.; Bernard, Y. A.; Berquist, E. J.; Burton, H. G. A.; Carreras, A.; Carter-Fenk, K.; Chakraborty, R.; Chien, A. D.; Closser, K. D.; Cofer-Shabica, V.; Dasgupta, S.; de Wergifosse, M.; Deng, J.; Diedenhofen, M.; Do, H.; Ehlert, S.; Fang, P.-T.; Fatehi, S.; Feng, Q.; Friedhoff, T.; Gayvert, J.; Ge, Q.; Gidofalvi, G.; Goldey, M.; Gomes, J.; González-Espinoza, C. E.; Gulania, S.; Gunina, A. O.; Hanson-Heine, M. W. D.; Harbach, P. H. P.; Hauser, A.; Herbst, M. F.; Hernández Vera, M.; Hodecker, M.; Holden, Z. C.; Houck, S.; Huang, X.; Hui, K.; Huynh, B. C.; Ivanov, M.; Jász, Á.; Ji, H.; Jiang, H.; Kaduk, B.; Kähler, S.; Khistyaev, K.; Kim, J.; Kis, G.; Klunzinger, P.; Koczor-Benda, Z.; Koh, J. H.; Kosenkov, D.; Koulias, L.; Kowalczyk, T.; Krauter, C. M.; Kue, K.; Kunitsa, A.; Kus, T.; Ladjánszki, I.; Landau, A.; Lawler, K. V.; Lefrancois, D.; Lehtola, S.; Li, R. R.; Li, Y.-P.; Liang, J.; Liebenthal, M.; Lin, H.-H.; Lin, Y.-S.; Liu, F.; Liu, K.-Y.; Loipersberger, M.; Luenser, A.; Manjanath, A.; Manohar, P.; Mansoor, E.; Manzer, S. F.; Mao, S.-P.; Marenich, A. V.; Markovich, T.; Mason, S.; Maurer, S. A.; McLaughlin, P. F.; Menger, M. F. S. J.; Mewes, J.-M.; Mewes, S. A.; Morgante, P.; Mullinax, J. W.; Oosterbaan, K. J.; Paran, G.; Paul, A. C.; Paul, S. K.; Pavošević, F.; Pei, Z.; Prager, S.; Proynov, E. I.; Rák, Á.; Ramos-Cordoba, E.; Rana, B.; Rask, A. E.; Rettig, A.; Richard, R. M.; Rob, F.; Rossomme, E.; Scheele, T.; Scheurer, M.; Schneider, M.; Sergueev, N.; Sharada, S. M.; Skomorowski, W.; Small, D. W.; Stein, C. J.; Su, Y.-C.; Sundstrom, E. J.; Tao, Z.; Thirman, J.; Tornai, G. J.; Tsuchimochi, T.; Tubman, N. M.; Veccham, S. P.; Vydrov, O.; Wenzel, J.; Witte, J.; Yamada, A.; Yao, K.; Yeganeh, S.; Yost, S. R.; Zech, A.; Zhang, I. Y.; Zhang, X.; Zhang, Y.; Zuev, D.; Aspuru-Guzik, A.; Bell, A. T.; Besley, N. A.; Bravaya, K. B.; Brooks, B. R.; Casanova, D.; Chai, J.-D.; Coriani, S.; Cramer, C. J.; Cserey, G.; DePrince, A. E., III; DiStasio, R. A., Jr.; Dreuw, A.; Dunietz, B. D.; Furlani, T. R.; Goddard, W. A., III; Hammes-Schiffer, S.; Head-Gordon, T.; Hehre, W. J.; Hsu, C.-P.; Jagau, T.-C.; Jung, Y.; Klamt, A.; Kong, J.; Lambrecht, D. S.; Liang, W.; Mayhall, N. J.; McCurdy, C. W.; Neaton, J. B.; Ochsenfeld, C.; Parkhill, J. A.; Peverati, R.; Rassolov, V. A.; Shao, Y.; Slipchenko, L. V.; Stauch, T.; Steele, R. P.; Subotnik, J. E.; Thom, A. J. W.; Tkatchenko, A.; Truhlar, D. G.; Van Voorhis, T.; Wesolowski, T. A.; Whaley, K. B.; Woodcock, H. L., III; Zimmerman, P. M.; Faraji, S.; Gill, P. M. W.; Head-Gordon, M.; Herbert, J. M.; Krylov, A. I., Software for the frontiers of quantum chemistry: An overview of developments in the Q-Chem 5 package. *J. Chem. Phys.* **2021,** *155* (8).
58. Noh, H.; Cui, Y.; Peters, A. W.; Pahls, D. R.; Ortuño, M. A.; Vermeulen, N. A.; Cramer, C. J.; Gagliardi, L.; Hupp, J. T.; Farha, O. K., An Exceptionally Stable Metal–Organic Framework Supported Molybdenum(VI) Oxide Catalyst for Cyclohexene Epoxidation. *J. Am. Chem. Soc.* **2016,** *138* (44), 14720-14726.
59. Baker, J., An algorithm for the location of transition states. *J. Comput. Chem.* **1986,** *7* (4), 385-395.
60. Van Voorhis, T.; Head-Gordon, M., A geometric approach to direct minimization. *Mol. Phys.* **2002,** *100* (11), 1713-1721.
61. Ghuffar, H. A.; Noh, H., Lithium-Coupled Electron Transfer Reactions of Nano-Confined WO_x within Zr-Based Metal-Organic Framework. *Frontiers in Chemistry* **2024**, **DOI:** 10.3389/fchem.2024.1427536.
62. (a) Fourmond, V.; Jacques, P.-A.; Fontecave, M.; Artero, V., H2 Evolution and Molecular Electrocatalysts: Determination of Overpotentials and Effect of Homoconjugation. *Inorg. Chem.* **2010,** *49* (22), 10338-10347. (b) Fourmond, V.; Jacques, P.-A.; Fontecave, M.; Artero, V., Correction to H_2 Evolution and Molecular Electrocatalysts: Determination of Overpotentials and Effect of Homoconjugation. *Inorg. Chem.* **2015,** *54* (2), 704-704. .
63. Fish, J. R.; Swarts, S. G.; Sevilla, M. D.; Malinski, T., Electrochemistry and spectroelectrochemistry of nitroxyl free radicals. *J. Phys. Chem.* **1988,** *92* (13), 3745-3751.
64. Nutting, J. E.; Rafiee, M.; Stahl, S. S., Tetramethylpiperidine N-Oxyl (TEMPO), Phthalimide N-Oxyl (PINO), and Related N-Oxyl Species: Electrochemical Properties and Their Use in Electrocatalytic Reactions. *Chem. Rev.* **2018,** *118* (9), 4834-4885.
65. Azimzadeh Sani, M.; Tschulik, K., Unveiling colloidal nanoparticle properties and interactions at a single entity level. *Curr. Opin. Electrochem.* **2023,** *37*, 101195.
66. Lucas, I. T.; Dubois, E.; Chevalet, J.; Durand-Vidal, S., Reactivity of nanocolloidal particles γ-Fe2O3 at the charged interfaces Part 1. The approach of particles to an electrode. *Phys. Chem. Chem. Phys.* **2008,** *10* (22), 3263-3273.
67. Ma, H.; Chen, J.-F.; Wang, H.-F.; Hu, P.-J.; Ma, W.; Long, Y.-T., Exploring dynamic interactions of single nanoparticles at interfaces for surface-confined electrochemical behavior and size measurement. *Nat. Commun.* **2020,** *11* (1), 2307.
68. Ho, W. H.; Li, S.-C.; Wang, Y.-C.; Chang, T.-E.; Chiang, Y.-T.; Li, Y.-P.; Kung, C.-W., Proton-Conductive Cerium-Based Metal–Organic Frameworks. *ACS Appl. Mater. Interfaces* **2021,** *13* (46), 55358-55366.
69. Wang, H.; Zhu, Q.-L.; Zou, R.; Xu, Q., Metal-Organic Frameworks for Energy Applications. *Chem* **2017,** *2* (1), 52-80.
70. Usov, P. M.; Huffman, B.; Epley, C. C.; Kessinger, M. C.; Zhu, J.; Maza, W. A.; Morris, A. J., Study of Electrocatalytic Properties of Metal–Organic Framework PCN-223 for the Oxygen Reduction Reaction. *ACS Appl. Mater. Interfaces* **2017,** *9* (39), 33539-33543.
71. Bagherzadeh, M.; Safarkhani, M.; Kiani, M.; Radmanesh, F.; Daneshgar, H.; Ghadiri, A. M.; Taghavimandi, F.; Fatahi, Y.; Safari-Alighiarloo, N.; Ahmadi, S.; Rabiee, N., MIL-125-based nanocarrier decorated with Palladium complex for targeted drug delivery. *Sci. Rep.* **2022,** *12* (1), 12105.
72. Howarth, A. J.; Liu, Y.; Li, P.; Li, Z.; Wang, T. C.; Hupp, J. T.; Farha, O. K., Chemical, thermal and mechanical stabilities of metal–organic frameworks. *Nat. Rev. Mater.* **2016,** *1* (3), 15018.
73. Johansson, E.; Boettcher, S. W.; O'Leary, L. E.; Poletayev, A. D.; Maldonado, S.; Brunschwig, B. S.; Lewis, N. S., Control of the pH-Dependence of the Band Edges of Si(111) Surfaces Using Mixed Methyl/Allyl Monolayers. *J. Phys. Chem. C* **2011,** *115* (17), 8594-8601.
74. Brown, E. S.; Peczonczyk, S. L.; Wang, Z.; Maldonado, S., Photoelectrochemical Properties of CH_3-Terminated p-Type GaP(111)A. *J. Phys. Chem. C* **2014,** *118* (22), 11593-11600.
75. Mian, M. R.; Wang, X.; Wang, X.; Kirlikovali, K. O.; Xie, H.; Ma, K.; Fahy, K. M.; Chen, H.; Islamoglu, T.; Snurr, R. Q.; Farha, O. K., Structure–Activity Relationship Insights for Organophosphonate Hydrolysis at Ti(IV) Active Sites in Metal–Organic Frameworks. *J. Am. Chem. Soc.* **2023,** *145* (13), 7435-7445.
76. Warburton, R. E.; Mayer, J. M.; Hammes-Schiffer, S., Proton-Coupled Defects Impact O–H Bond Dissociation Free Energies on Metal Oxide Surfaces. *J. Phys. Chem. Lett.* **2021,** *12* (40), 9761-9767.
77. Lyon, L. A.; Hupp, J. T., Energetics of the Nanocrystalline Titanium Dioxide/Aqueous Solution Interface: Approximate Conduction Band Edge Variations between $H_0 = -10$ and $H_- = +26$. *J. Phys. Chem. B* **1999,** *103* (22), 4623-4628.
78. Luo, Y.-R., *Comprehensive Handbook of Chemical Bond Energies*. CRC Press: Boca Raton, FL, 2007.
79. For molecules of similar size and polarity like methanol and formaldehyde, entropic change upon redox reaction is minimal even in polar solvents like H_2O; see ref. 7 for more details. .
80. Bueken, B.; Vermoortele, F.; Vanpoucke, D. E. P.; Reinsch, H.; Tsou, C.-C.; Valvekens, P.; De Baerdemaeker, T.; Ameloot, R.; Kirschhock, C. E. A.; Van Speybroeck, V.; Mayer, J. M.; De Vos, D., A Flexible Photoactive Titanium Metal–Organic Framework Based on a $[Ti^{IV3}(\mu_3\text{-}O)(O)_2(COO)_6]$ Cluster. *Angew. Chem. Int. Ed.* **2015,** *54* (47), 13912-13917.
81. Mancuso, J. L.; Fabrizio, K.; Brozek, C. K.; Hendon, C. H., On the limit of proton-coupled electronic doping in a Ti(IV)-containing MOF. *Chem. Sci.* **2021,** *12* (35), 11779-11785.

82. Wiedner, E. S.; Chambers, M. B.; Pitman, C. L.; Bullock, R. M.; Miller, A. J. M.; Appel, A. M., Thermodynamic Hydricity of Transition Metal Hydrides. *Chem. Rev.* **2016,** *116* (15), 8655-8692.
83. Pegis, M. L.; Roberts, J. A. S.; Wasylenko, D. J.; Mader, E. A.; Appel, A. M.; Mayer, J. M., Standard Reduction Potentials for Oxygen and Carbon Dioxide Couples in Acetonitrile and *N,N*-Dimethylformamide. *Inorg. Chem.* **2015,** *54* (24), 11883-11888.
84. Chen, Y.; Chen, H.; Tian, H., Immobilization of a cobalt catalyst on fullerene in molecular devices for water reduction. *Chem. Commun.* **2015,** *51* (57), 11508-11511.
85. Connelly, N. G.; Geiger, W. E., Chemical Redox Agents for Organometallic Chemistry. *Chem. Rev.* **1996,** *96* (2), 877-910.
86. Aranzaes, J. R.; Daniel, M.-C.; Astruc, D., Metallocenes as references for the determination of redox potentials by cyclic voltammetry — Permethylated iron and cobalt sandwich complexes, inhibition by polyamine dendrimers, and the role of hydroxy-containing ferrocenes. *Can. J. Chem.* **2006,** *84* (2), 288-299.
87. Shalev, H.; Evans, D. H., Solvation of anion radicals: gas-phase versus solution. *J. Am. Chem. Soc.* **1989,** *111* (7), 2667-2674.
88. Parker, V. D.; Handoo, K. L.; Roness, F.; Tilset, M., Electrode potentials and the thermodynamics of isodesmic reactions. *J. Am. Chem. Soc.* **1991,** *113* (20), 7493-7498.
89. For molecular species and NiO, BDFEs have been shown to be independent of solvents. However, this is yet to be proven for Ti-MIL-125, and hence eq. 16' is considered a chemically distinct reaction as to eq. 16. See ref. 7 and 11 for more details.
90. Kütt, A.; Tshepelevitsh, S.; Saame, J.; Lõkov, M.; Kaljurand, I.; Selberg, S.; Leito, I., Strengths of Acids in Acetonitrile. *Eur. J. Org. Chem.* **2021,** *2021* (9), 1407-1419.
91. Rossini, E.; Bochevarov, A. D.; Knapp, E. W., Empirical Conversion of pKa Values between Different Solvents and Interpretation of the Parameters: Application to Water, Acetonitrile, Dimethyl Sulfoxide, and Methanol. *ACS Omega* **2018,** *3* (2), 1653-1662.
92. Izutsu, K., Acid-Base Reactions in Non-Aqueous Solvents. In *Electrochemistry in Nonaqueous Solutions*, Wiley-VCH: Weinheim, 2002; pp 59-83.
93. Kresse, G.; Furthmüller, J., Efficiency of ab-initio total energy calculations for metals and semiconductors using a plane-wave basis set. *Comp. Mater. Sci.* **1996,** *6* (1), 15-50.
94. Kresse, G.; Furthmüller, J., Efficient iterative schemes for ab initio total-energy calculations using a plane-wave basis set. *Phys. Rev. B* **1996,** *54* (16), 11169-11186.
95. Kresse, G.; Hafner, J., Ab initio molecular dynamics for liquid metals. *Phys. Rev. B* **1993,** *47* (1), 558-561.
96. Yin, X.-L.; Calatayud, M.; Qiu, H.; Wang, Y.; Birkner, A.; Minot, C.; Wöll, C., Diffusion versus Desorption: Complex Behavior of H Atoms on an Oxide Surface. *ChemPhysChem* **2008,** *9* (2), 253-256.
97. Islam, M. M.; Calatayud, M.; Pacchioni, G., Hydrogen Adsorption and Diffusion on the Anatase TiO_2(101) Surface: A First-Principles Investigation. *J. Phys. Chem. C* **2011,** *115* (14), 6809-6814.
98. Gileadi, E., Adsorption in Electrochemistry. In *Electrosorption*, Gileadi, E., Ed. Springer: Boston, MA, 1967; Vol. 1, pp 1-18.
99. Gileadi, E., Chapter 19: Adsorption isotherms for intermediates formed by charge transfer. In *Electrode Kinetics for Chemists, Chemical Engineers and Materials Scientists*, VCH Publishers: 1993; pp 261-280.
100. Whittaker, E. J. W.; Muntus, R., Ionic radii for use in geochemistry. *Geochim. Cosmochim. Acta* **1970,** *34* (9), 945-956.
101. Finklea, H. O., Titanium Dioxide (TiO_2) and Strontium Titanate ($SrTiO_3$). In *Semiconductor Electrodes*, Finklea, H. O., Ed. Elsevier: Amsterdam, 1988; pp 42-154.
102. Laviron, E., Surface linear potential sweep voltammetry: Equation of the peaks for a reversible reaction when interactions between the adsorbed molecules are taken into account. *J. Electroanal. Chem. Interfacial Electrochem.* **1974,** *52* (3), 395-402.
103. Laviron, E., The use of linear potential sweep voltammetry and of a.c. voltammetry for the study of the surface electrochemical reaction of strongly adsorbed systems and of redox modified electrodes. *J. Electroanal. Chem. Interfacial Electrochem.* **1979,** *100* (1), 263-270.
104. Shen, G.; Zhang, X. H.; Ming, Y.; Zhang, L.; Zhang, Y.; Hu, J., Photocatalytic Induction of Nanobubbles on TiO_2 Surfaces. *J. Phys. Chem. C* **2008,** *112* (11), 4029-4032.
105. Fiaz, M.; Athar, M., Modification of MIL-125(Ti) by Incorporating Various Transition Metal Oxide Nanoparticles for Enhanced Photocurrent during Hydrogen and Oxygen Evolution Reactions. *ChemistrySelect* **2019,** *4* (29), 8508-8515.
106. Kavun, V.; Uslamin, E.; van der Linden, B.; Canossa, S.; Goryachev, A.; Bos, E. E.; Garcia Santaclara, J.; Smolentsev, G.; Repo, E.; van der Veen, M. A., Promoting Photocatalytic Activity of NH_2-MIL-125(Ti) for H_2 Evolution Reaction through Creation of Ti^{III}- and Co^{I}-Based Proton Reduction Sites. *ACS Appl. Mater. Interfaces* **2023,** *15* (47), 54590-54601.
107. He, Y.; Lv, T.; Xiao, B.; Liu, B.; Zhou, T.; Zhang, J.; Zhang, Y.; Zhang, G.; Liu, Q., Research progress of MIL-125 and its modifications in photocatalytic hydrogen evolution. *J. Mater. Chem. C* **2023,** *11* (21), 6800-6818.
108. Lindgren, P.; Kastlunger, G.; Peterson, A. A., A Challenge to the G ~ 0 Interpretation of Hydrogen Evolution. *ACS Catal.* **2020,** *10* (1), 121-128.